Energy Conversion and Management 199 (2019) 111958

Contents lists available at ScienceDirect

Energy Conversion and Management

journal homepage: www.elsevier.com/locate/enconman

The energy flow method for modeling and optimization of Organic Rankine Cycle (ORC) systems

Guangfeng Shen, Fang Yuan*, Yi Li, Wei Liu

School of Energy and Power Engineering, Huazhong University of Science and Technology, Wuhan 430074, China

ARTICLE INFO

Keywords:
ORC
Thermal resistance
Power source
Energy flow model
Optimization

ABSTRACT

This contribution constructs the energy flow model for an ORC system, which synthetically considers fluid characteristics and governing laws of heat transfer and thermodynamic. Then, combined the Kirchhoff's law with the thermodynamic constraints, a group of mathematical equations is obtained. It not only reveals both system topological structure and the component characteristics, but also connects the system output to the boundary conditions, the structural parameters and the operating parameters. Finally, operation optimizations for a certain ORC system are implemented via Genetic Algorithm (GA). Two sets of Pareto frontiers with different heat source conditions are obtained. The results show that with a 16 K increment of heat source temperature, the net power output and thermal efficiency will increase by 84% and 25%, respectively. In the other hand, the heat source flow rate shows limited impact on optimizations. Besides, design optimizations with the objective of minimizing required total thermal conductance are also conducted. It is concluded that enlarging net power output by 14.9% leads to an increase in the total thermal conductance by 54.3% and a decrease in the corresponding working fluid flow rate by 8.7%. Moreover, the operating parameters related to condenser other than evaporator remarkably influence the optimizations, and the characteristic temperatures vary with different conditions in each optimization. Therefore, the proposed method without fixed PPTD or condensation temperature is more flexible to both modeling and optimization.

1. Introduction

Energy crisis caused by fossil fuel consumption and low energy utilization efficiency, has drawn continuous and worldwide attention in both engineering and scientific fields. The Organic Rankine Cycle (ORC), as one of the promising technologies for recovering waste heat in sustainable energy utilization systems [1,2] and conventional industrial processes [3–5], is environment-friendly and adaptive to low-grade heat sources [6], compared with the conventional Steam Rankine Cycle. Therefore, it has obtained a dramatic growth in applications over the past several decades.

Until now, researches still put huge effort into working fluid selection and parametric study, because they both have a direct and significant impact on the performance of ORC systems. Generally, working fluids including pure fluids and zeotropic mixtures can be categorized into dry fluids, wet fluids and isentropic fluids based on the slopes of saturated vapor line [7]. Meanwhile, the major operating parameters studied include evaporation temperature [8], heat source temperature [9,10], degree of superheat [11–13], pinch point temperature differences (PPTD) [14], mass flow rates [15], etc. Scientists commonly optimize system by analyzing the heat transfer, thermodynamic and economic performance with different working fluids and operating conditions. In addition, various optimization strategies have been developed for further improving system performance. For instance, different cycle configurations such as single stage regenerative ORC [16], double stage regenerative ORC [17], ORC with recuperator [18], dual loop ORC [19] have been established and studied. Optimizations with different objectives like net power output [15], thermal efficiency [20] and exergy efficiency [21] have also been implemented, applying different optimization algorithms such as ROSENB optimization algorithm [15], firefly algorithm [22], Exhaustive search [23] and genetic algorithm (GA) [24–26].

Experimental study [27–29] and theoretical analysis [30–32] are two major research methods for analyzing and optimizing system. Comparing with the former, the latter is more flexible and costs lower. Modelling, as the basis of theoretical analysis, is crucial to calculation. For simplicity, researchers usually fix some characteristic parameters such as the pinch point temperature difference (PPTD) [33,34] and the condensation temperature or pressure [7,8] to calculate each component in turn by basic physical equations, so as to obtain the system

* Corresponding author.
E-mail address: yuanf@hust.edu.cn (F. Yuan).

https://doi.org/10.1016/j.enconman.2019.111958
Received 25 April 2019; Received in revised form 2 August 2019; Accepted 18 August 2019

Nomenclature

c_p	constant pressure specific heat, J kg^{-1} K^{-1}
g	gravitational acceleration, m s^{-2}
H	pump head, m
h	the specific enthalpy, J kg^{-1}
KA	thermal conductance, W K^{-1}
m	mass flow rate, kg s^{-1}
P	pressure, kPa
Q	heat transfer rate, W
R	inlet temperature difference-based thermal resistance, K W^{-1}
s	specific entropy, J kg^{-1} K^{-1}
T	temperature, K
W	power, W
γ	the specific latent heat, J kg^{-1}
ε	additive thermo-motive force, K
η	thermal efficiency

Subscript

c	condenser
e	evaporator
ex	expander
f	working fluid
h	heat source
i	inlet
net	net
o	outlet
p	pump
pc	pre-cooling
ph	pre-heating
sh	super-heating
w	cooling water

output. It is noticed that heat transfer areas of both condenser and evaporator are calculated and vary with different conditions. Therefore, this method benefits preliminary design, but it is not convenient to a certain system with specific condenser and evaporator. The optimization results based on this method maybe not suitable for a certain system. If a prescribed evaporator and condenser have been considered, the iteration procedure is indispensable. For instance, Kim et al. [35] used ε-NTU method to handle heat transfer process in the condenser and evaporator, and assumed one evaporation temperature to start the iteration. Obviously, iteration process would remarkably increase the complexity of model especially for the multi-stage or combined systems. In addition, all modeling methods mentioned above are component-oriented, i.e., They analyze each component in the system according to the governing equations, simplified mathematical relations or empirical correlations and then solve the equations with or without iteration. It will introduce abundant variables as intermediate temperatures, and increase the computational burden especially for complex systems.

In recent years, Chen et al. [36] derived the entransy dissipation-based thermal resistance for heat exchanger on the basis of the entransy theory [37]. Then, inspired by the thermal-electrical analogy, Chen and his colleagues proposed an energy flow method to analyze and optimize various thermal systems, including absorption energy storage system [38], district heating system [39], building heat transport and gas refrigeration system [40] and integrated electric-thermal energy system [41]. This method pays more attention to energy transport through the whole system. Obviously, it is a system-oriented method, which could avoid the problems resulted from the conventional modelling method. However, the energy flow method for the ORC system taking variable fluid characteristics into consideration, is still worth investigating further.

This study first constructs an energy flow model consisting of thermal resistances, power sources and additive thermo-motive forces for a typical ORC system. Then, a group of equations that represents the topological structure of the ORC system is deduced, according to the Kirchhoff's law in electrical circuit theory. Combined with the thermodynamic constraints and characteristics of working fluid, modeling of the ORC system is accomplished. Finally, two typical optimizations for the ORC system are conducted via Genetic Algorithm to show the applications and advantages of the newly proposed modelling method. The influences of some characteristic parameters on system optimization are also discussed.

2. System description

Fig. 1(a) shows the schematic of a typical ORC system, which is mainly composed of four components as an evaporator, an expander, a condenser and a working fluid pump. Its corresponding *T-s* diagram is shown in Fig. 1(b), where $T_{h,i}$ and $T_{w,i}$ are the inlet temperatures of heat source and cooling water, respectively. In the evaporator, the liquid working fluid at state 1 is evaporated and becomes superheated vapor at state 2 by absorbing heat from the heat source (isobaric heat absorption process 1 → 2). Then, the vapor with high temperature and pressure passes through the expander to drive electricity generator and

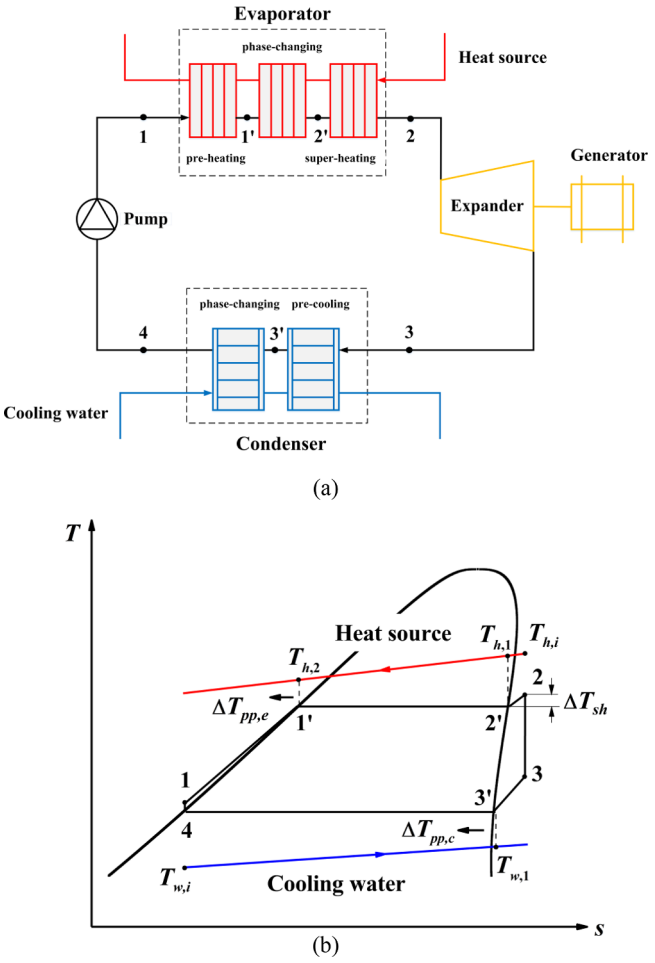

Fig. 1. Schematic of a typical ORC system (a) and its corresponding *T-s* diagram (b).

exits at state 3 (isentropic expansion process 2 → 3). Afterwards, in the condenser, the vapor is re-condensed to liquid state 4 by emitting heat to the cooling water (isobaric heat rejection process 3 → 4). Finally, the liquid phase working fluid is compressed to high pressure at state 1 via the working fluid pump and re-enters into the evaporator to start another cycle (isentropic compression process 4 → 1). In brief, with the aid of the working fluid pump, the system could obtain expansion work by absorbing heat from the heat source and then releasing heat to the cooling water.

It is worth to mention that working fluid experiences such three states in the evaporator as liquid, liquid-vapor and supper-heated vapor. Therefore, the evaporator could be considered as three series-connected counter-flow heat exchangers, namely, a pre-heating heat exchanger, a hot-side phase-changing heat exchanger and a super-heating heat exchanger. Similarly, since the state of working fluid flowing through the condenser varies from super-heated vapor to vapor-liquid, it could be regarded as two series-connected counter-flow heat exchangers, namely, a pre-cooling heat exchanger and a cold-side phase-changing heat exchanger.

Furthermore, some assumptions are made to simplify the analysis: (1) The system is in a steady state; (2) Pressure drops in the connecting pipelines and heat exchangers are ignored compared with that in the expander; (3) The expansion and compression processes are both isentropic; (4) The specific heat capacity of working fluid in each single-phase heat exchanger remains constant.

3. Energy flow model of the ORC system

The ORC system consists of both heat transfer and thermodynamic processes involving three fluids. Thus, the newly proposed modelling method will deal with these two different processes individually from the perspective of energy flow.

3.1. Energy flow analysis of ORC system

Inspired by the analogy of heat transfer with electrical conduction, Chen et al. [36] proposed a thermal resistance model for heat exchanger, as shown in Fig. 2(a). Applying the Ohm's law, the heat transfer rate Q_e for each heat transfer process in the evaporator then could be expressed as

$$Q_e = \frac{T_{h,i} - T_{f,i}}{R_e}, \tag{1}$$

where $T_{h,i} - T_{f,i}$ stands for the temperature difference between inlet temperatures of heat source and working fluid, i.e., the maximum potential difference for heat transfer process. R_e represents the inlet temperature difference-based thermal resistance. For a counter-flow heat exchanger, it could be expressed as

$$R_e = \frac{m_f c_{p,f} \exp\left(\frac{KA}{m_h c_{p,h}}\right) - m_h c_{p,h} \exp\left(\frac{KA}{m_f c_{p,f}}\right)}{m_h c_{p,h} m_f c_{p,f} \left[\exp\left(\frac{KA}{m_h c_{p,h}}\right) - \exp\left(\frac{KA}{m_f c_{p,f}}\right)\right]}, \tag{2}$$

where m and c_p represent the mass flow rate and the specific heat capacity, respectively. KA denotes the thermal conductance of the heat exchanger, i.e., the product of the heat transfer coefficient (K) and the heat transfer area (A). Subscripts h and f stand for the heat source and working fluid, respectively. Apparently, the thermal resistance only relies on thermal conductance and mass flow rate, i.e., the structural and the operating parameters of the heat exchanger.

Similarly, the heat transfer rate Q_c for each heat transfer process in the condenser could be expressed as

$$Q_c = \frac{T_{f,i} - T_{w,i}}{R_c}, \tag{3}$$

where $T_{f,i} - T_{w,i}$ stands for the temperature difference between inlet temperatures of working fluid and cooling water. The corresponding inlet temperature difference-based thermal resistance R_c could be written as

$$R_c = \frac{m_w c_{p,w} \exp\left(\frac{KA}{m_f c_{p,f}}\right) - m_f c_{p,f} \exp\left(\frac{KA}{m_w c_{p,w}}\right)}{m_f c_{p,f} m_w c_{p,w} \left[\exp\left(\frac{KA}{m_f c_{p,f}}\right) - \exp\left(\frac{KA}{m_w c_{p,w}}\right)\right]}, \tag{4}$$

where subscript w stands for the cooling water. Thus, via the thermal resistance model, the heat transfer process between hot-side fluid and cold-side fluid could be theoretically characterized. This model directly establishes the relation between the nodal temperatures (inlet temperatures) and the heat transfer rate, namely, nodal potentials and flow rate. Moreover, it also describes the relation of heat flow rate and the thermal conductance, namely, the performance of evaporator and condenser and their structures.

On the other hand, the temperature variation for working fluid or cooling water (heat source) caused by heat transfer process could be characterized by an additive thermo-motive force shown in Fig. 2(b). According to the energy conservation equation, it could be expressed as

$$\varepsilon = T_{h,i} - T_{h,o} = \frac{Q}{mc_p}, \tag{5}$$

where subscripts o and i stand for outlet and inlet, respectively. ε always keeps positive and could reflect the increment of temperature potential like a voltage source in the electrical circuit.

Different from the heat transfer processes, the thermodynamic processes in the cycle only involve working fluid. Then, external power sources shown in Fig. 2(c) and (d), like current sources in the electrical circuit, are proposed to depict the work input from the working fluid pump and the work output from the expander. As a result of power sources, the temperature of working fluid will either increase or decrease. Then, the temperature variation of working fluid due to the working fluid pump could also use an additive thermo-motive force to represent, that is

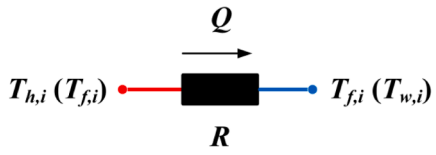

(a) Thermal resistance

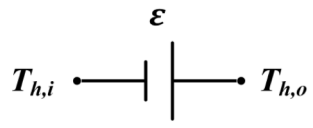

(b) Additive thermo-motive force

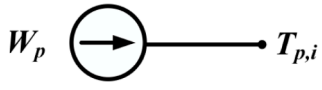

(c) Input power source

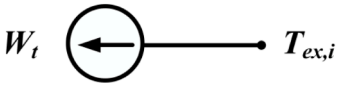

(d) Output power source

Fig. 2. Four basic analogous electrical components for the energy flow model.

$$\varepsilon_p = T_{p,o} - T_{p,i}, \tag{6}$$

where subscript p stands for the working fluid pump.

Afterwards, taking thermal resistance, additive thermal-motive force, input power source and output power source introduced above as the basic components, the energy flow model of ORC system could be constructed by connecting the state points with the same temperature, as shown in Fig. 3.

In the figure, different line colors are used for distinguishing different working medium. Here, the red line, the blue line and the black line stand for the heat source, the cooling water, and the working fluid, respectively. Line 3-3′-4-1-1′-2′-2 represents the states of working fluid in the cycle experienced in turn, corresponding to Fig. 1. Considering the energy flow model for series-connected heat exchanger network [36], the evaporator could be characterized by three thermal resistances in parallel, namely, $R_{e,1}$, $R_{e,2}$ and $R_{e,3}$, while $Q_{e,1}$, $Q_{e,2}$ and $Q_{e,3}$ are the corresponding heat transfer rates. The condenser could be characterized by two thermal resistances in parallel, namely, $R_{c,1}$ and $R_{c,2}$, while $Q_{c,1}$ and $Q_{c,2}$ are their corresponding heat transfer rates.

Moreover, ε_c, $\varepsilon_{e,1}$ and $\varepsilon_{e,2}$ represent the temperature variations of working fluid in the pre-cooling process, pre-heating process and super-heating process, respectively; ε_w stands for the temperature variation of the cooling water through the cold-side phase-changing heat exchanger; $\varepsilon_{h,1}$ and $\varepsilon_{h,2}$ are the temperature variations of heat source through the super-heating heat exchanger and hot-side phase-changing heat exchanger, respectively. $T_{w,1}$ is the outlet temperature of cooling water in the cold-side phase-changing heat exchanger; $T_{h,1}$ and $T_{h,2}$ are the heat source outlet temperatures of the super-heating heat exchanger and the hot-side phase-changing heat exchanger, respectively; $T_{ex,i}$ and $T_{ex,o}$ represent the inlet and outlet temperature of the expander, respectively; T_c and T_e represent the condensation and evaporation temperature, respectively; while, $T_{p,o}$ represents the outlet temperature of the working fluid pump. W_p and W_t are the power consumption of the working fluid pump and the work output from the expander, respectively.

The energy flow model simultaneously describes the heat transfer and the heat-work conversion processes in the ORC system and indicates the connection relations between each component as well. It is analogous to an electrical network, compared with the conventional component-oriented model. Therefore, Kirchhoff's law, the classical analysis method for DC circuit, could be applied to establish the mathematical relation of this energy flow model.

3.2. Modeling of the ORC system

For a certain ORC system with a prescribed evaporator and condenser, the system boundary conditions (i.e., inlet temperatures $T_{h,i}$ and $T_{w,i}$, and mass flow rates m_h and m_w), and the operating conditions (i.e., mass flow rate of working fluid m_f and degree of superheat ΔT_{sh}) determine each nodal temperature T_c, T_e, $T_{p,o}$, $T_{ex,i}$ and $T_{ex,o}$ in the cycle, the work input W_p and the work output W_t. Therefore, the intermediate temperatures are not indispensable for modelling. Based on the Kirchhoff's voltage law, the mathematical equations without intermediate temperatures could be obtained to depict the system topological relation,

$$T_{w,i} + \varepsilon_w + Q_{c,1}R_{c,1} - \varepsilon_c + \varepsilon_p + Q_{e,1}R_{e,1} + \varepsilon_{h,2} + \varepsilon_{h,1} = T_{h,i}, \tag{7}$$

$$T_{w,i} + Q_{c,2}R_{c,2} + \varepsilon_p + Q_{e,1}R_{e,1} + \varepsilon_{h,2} + \varepsilon_{h,1} = T_{h,i}, \tag{8}$$

$$T_{w,i} + \varepsilon_w + Q_{c,1}R_{c,1} - \varepsilon_c + \varepsilon_p + \varepsilon_{e,1} + Q_{e,2}R_{e,2} + \varepsilon_{h,1} = T_{h,i}, \tag{9}$$

$$T_{w,i} + Q_{c,2}R_{c,2} + \varepsilon_p + \varepsilon_{e,1} + Q_{e,2}R_{e,2} + \varepsilon_{h,1} = T_{h,i}, \tag{10}$$

$$T_{w,i} + \varepsilon_w + Q_{c,1}R_{c,1} - \varepsilon_c + \varepsilon_p + \varepsilon_{e,1} + Q_{e,3}R_{e,3} = T_{h,i}, \tag{11}$$

$$T_{w,i} + Q_{c,2}R_{c,2} + \varepsilon_p + \varepsilon_{e,1} + Q_{e,3}R_{e,3} = T_{h,i}, \tag{12}$$

where the expressions of additive thermal-motive forces caused by heat transfer are,

$$\varepsilon_w = T_{w,1} - T_{w,i} = \frac{Q_{c,2}}{m_w c_{p,w}}, \tag{13}$$

$$\varepsilon_{h,1} = T_{h,i} - T_{h,1} = \frac{Q_{e,3}}{m_h c_{p,h}}, \tag{14}$$

$$\varepsilon_{h,2} = T_{h,1} - T_{h,2} = \frac{Q_{e,2}}{m_h c_{p,h}}, \tag{15}$$

$$\varepsilon_c = T_{ex,o} - T_c = \frac{Q_{c,1}}{m_f c_{p,pc}}, \tag{16}$$

$$\varepsilon_{e,1} = T_e - T_{p,o} = \frac{Q_{e,1}}{m_f c_{p,ph}}, \tag{17}$$

$$\varepsilon_{e,2} = T_{ex,i} - T_e = \Delta T_{sh} = \frac{Q_{e,3}}{m_f c_{p,sh}}, \tag{18}$$

where subscripts w, h and f represent cooling water, heat source and working fluid, respectively; pc, ph and sh stand for the pre-cooling process of the condenser, the pre-heating process of the evaporator and the super-heating process of the evaporator, respectively.

Substituting the corresponding mass flow rate, specific heat capacity and thermal conductance of each heat exchanger into Eqs. (2) and (4), thermal resistances $R_{c,1}$, $R_{e,1}$ and $R_{e,3}$ will be obtained. Considering the evaporation and condensation process, thermal resistances of the cold-side and hot-side phase-changing heat exchangers could be simplified into

$$R_{c,2} = \frac{\exp[(KA)_{c,2}/m_w c_{p,w}]}{m_w c_{p,w}\exp[(KA)_{c,2}/m_w c_{p,w}] - m_w c_{p,w}}, \tag{19}$$

$$R_{e,2} = \frac{\exp[(KA)_{e,2}/m_h c_{p,h}]}{m_h c_{p,h}\exp[(KA)_{e,2}/m_h c_{p,h}] - m_h c_{p,h}}, \tag{20}$$

while, the corresponding heat transfer rates could be calculated by

$$Q_{c,2} = -m_f \gamma_c, \tag{21}$$

$$Q_{e,2} = m_f \gamma_e, \tag{22}$$

where γ_c and γ_e are the specific latent heats of working fluid at temperature T_c and T_e, respectively.

As mentioned above, the condenser could be considered as the combination of two series-connected heat exchangers, while the evaporator consists of three series-connected heat exchangers. Thus, the thermal conductance of the evaporator and the condenser could be expressed as

$$(KA)_{c,1} + (KA)_{c,2} = (KA)_c, \tag{23}$$

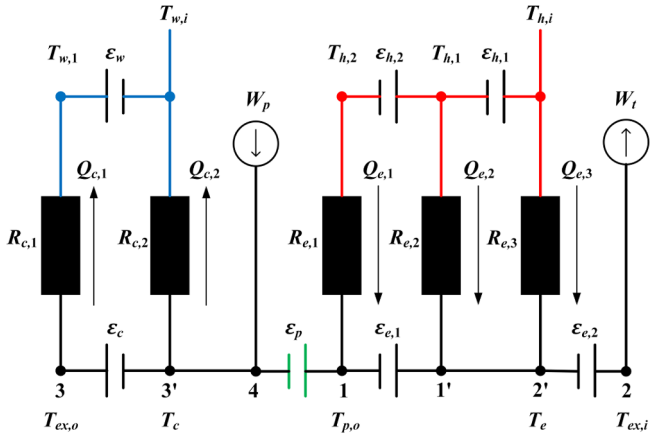

Fig. 3. The energy flow model of a typical ORC system.

$$(KA)_{e,1} + (KA)_{e,2} + (KA)_{e,3} = (KA)_e. \quad (24)$$

Besides, for the properties of working fluid in the phase-changing process are related to evaporation and condensation temperatures, the mathematical relation between T_c and T_e should also be characterized. From the energy flow model, there is

$$T_c + \varepsilon_p + \varepsilon_{e,1} = T_e. \quad (25)$$

Simultaneously solving Eqs. (7)–(12), (18) and (21)–(25), twelve variables in right side of the following equivalent mathematical relation could be obtained,

$$[T_{h,i},\ T_{w,i},\ m_h,\ m_w,\ m_f,\ (KA)_e,\ (KA)_c,\ \Delta T_{sh}] = f\begin{bmatrix} T_e,\ T_c,\ Q_{c,1},\ Q_{c,2},\ Q_{e,1},\ Q_{e,2},\ Q_{e,3}, \\ (KA)_{c,1},\ (KA)_{c,2},\ (KA)_{e,1},\ (KA)_{e,2},\ (KA)_{e,3} \end{bmatrix}, \quad (26)$$

where its left side is the input known working condition. It is clear that the energy flow model directly connects the energy input Q_e, the energy output Q_c and system boundary conditions, i.e., $T_{h,i}$, $T_{w,i}$, m_h and m_w, to the structural parameters, i.e., $(KA)_e$ and $(KA)_c$ and the operating parameters, i.e., m_f and ΔT_{sh}. It is a system-oriented modelling method, which concentrates on the overall energy transport law in the ORC system. Moreover, it is worth to mention that, both T_e and T_c in Eq. (26) are not the independent variables and they are only used to determine the thermodynamic properties of working fluid.

Afterwards, the temperature of working fluid entering into the expander $T_{ex,i}$ could be calculated by Eq. (18), and other intermediate temperatures could be obtained from the thermodynamic relation of working fluid in the database REFPROP 9.0,

$$T_{ex,o} = f(s_{ex,i},\ P_c), \quad (27)$$

$$T_{p,o} = f(s_{p,i},\ P_e), \quad (28)$$

where P_e and P_c are the evaporation and condensation pressure determined by T_e and T_c, respectively. s represents the specific entropy of working fluid. Then, for the heat-work conversion process, the work output from the expander could be calculated from the energy conservation equation,

$$W_t = m_f\,[h(P_e,\ T_{ex,i}) - h(P_c,\ T_{ex,o})], \quad (29)$$

where h stands for the specific enthalpy of working fluid, which depends on both pressure and temperature. Similarly, the power consumption of the working fluid pump is

$$W_p = m_f\,[h(P_e,\ T_{p,o}) - h(T_c)]. \quad (30)$$

The flow chart for solution scheme of the energy flow model is showed in Fig. 4. At the beginning of the iteration, we should assume T_e and T_c to initialize the thermodynamic properties of working fluid. Then, solving the equations achieved from the energy flow model, the system work output, thermal conductance allocations of evaporator and condenser as well as all intermediate temperatures could be obtained. At last, the update T_e and T_c will refresh the thermodynamic properties after each step of iteration until convergence. The relations of working fluid properties and state parameters could be obtained by the database REFPROP 9.0.

To sum up, compared with the traditional modelling method, the energy flow model has the following major advantages: (1) The intermediate temperatures in the system are not necessary for the iteration process, therefore, the number of variables and equations could be reduced to the maximum extent. (2) It describes the theoretical relation between each component in the system and reveals the component characteristic via thermal resistance model as well. (3) It is convenient to calculate and optimize a certain system with specific condenser and evaporator without fixing some characteristic temperatures in advance. Therefore, it is in favor of both operation optimization and preliminary design.

3.3. Model verification

In order to validate the reliability of the proposed energy flow model, Fig. 5 offers the comparisons of the thermal efficiency calculated by the energy flow model with the theoretical and numerical data in the literature [24], where R245fa is taken as the working fluid. The prescribed parameters such as inlet temperature, mass flow rate, PPTD and isentropic efficiency are listed in Table 1. The results show that the energy flow model has a good agreement with both theoretical data and numerical data, wherein, the maximum relative error is about 4.5% and 6.6%, respectively.

For further verification, the comparison of characteristic parameters calculated by the energy flow model with the experimental data in the literature [42] are also conducted, as listed in Table 3. The boundary and operating parameters of experimental model are listed in Table 2. The results could also demonstrate the validity of the energy flow model, wherein, the deviation of the work output is only 2.2%.

4. Optimizations and discussions

Generally speaking, optimization problems for an ORC system can be categorized into two types: i) Operation optimization, i.e., for a certain ORC system with specific components, optimize the allocation of the mass flow rates of heat source, working fluid and cooling water could obtain the maximum net power output or efficiency; ii) Design

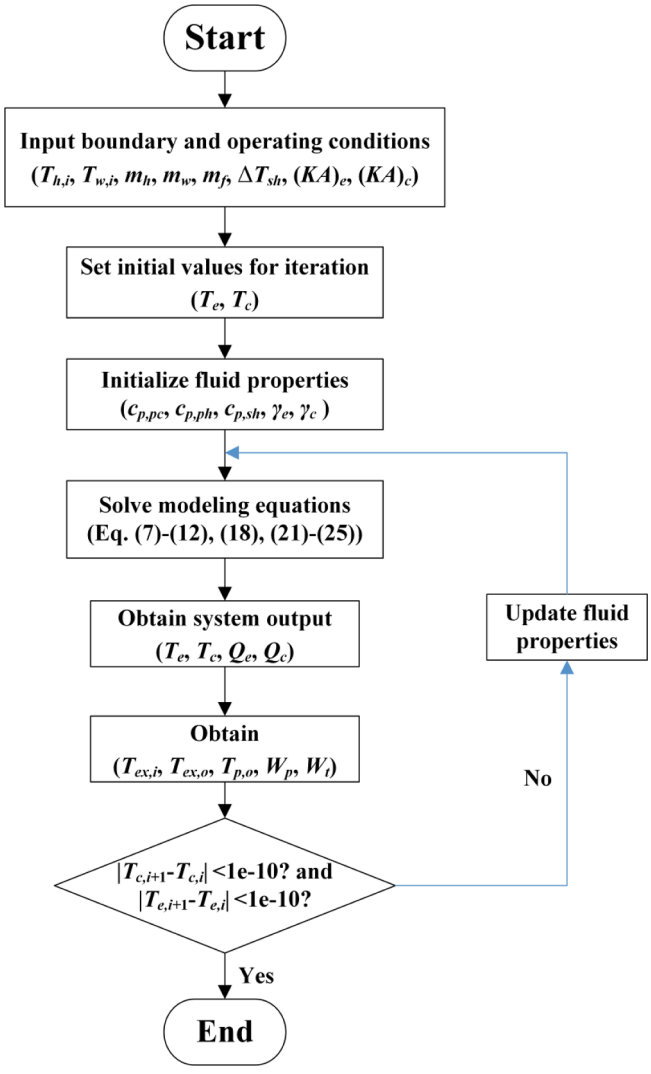

Fig. 4. The flow chat for solution scheme of the energy flow model.

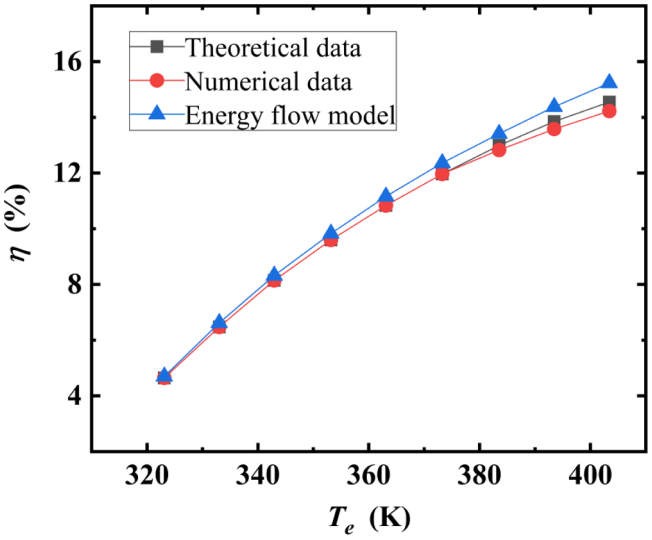

Fig. 5. The comparisons of thermal efficiency with the theoretical and numerical data in Ref. [24].

Table 1
The prescribed parameters of validation model.

Parameter	Symbol	Value/range
Inlet temperature of heat source, K	$T_{h,i}$	393
Mass flow rate of heat source, kg s^{-1}	m_h	30
Evaporation temperature, K	T_e	323–403
Condensation temperature, K	T_c	303
PPTD in evaporator, K	$\Delta T_{pp,e}$	5
PPTD in condenser, K	$\Delta T_{pp,c}$	5
Isentropic efficiency of working fluid pump	η_p	1
Isentropic efficiency of expander	η_{ex}	0.8

Table 2
The boundary and operating parameters of the experimental model.

Parameter	Symbol	Value
Inlet temperature of heat source, K	$T_{h,i}$	366.3
Mass flow rate of heat source, m^3 h^{-1}	m_h	4.2
Inlet temperature of cooling water, K	$T_{w,i}$	302.7
Mass flow rate of cooling water, m^3 h^{-1}	m_w	7.9
Mass flow rate of working fluid, kg s^{-1}	m_f	0.1048
Thermal conductance of evaporator, W K^{-1}	$(KA)_e$	7543
Thermal conductance of condenser, W K^{-1}	$(KA)_c$	3670
Degree of superheat, K	ΔT_{sh}	1.7
Isentropic efficiency of expander	η_{ex}	0.487

Table 3
The comparison of the energy flow model with the experimental data.

	W_t (W)	$T_{h,o}$ (K)	$T_{w,o}$ (K)	T_e (K)	T_c (K)
Ref. [42]	1450.5	361.86	304.86	362.15	309.15
Energy flow model	1418.3	361.59	304.86	362.18	309.20
Relative error	2.2e-2	−7.5e-4	4.3e-6	8.3e-5	1.6e-4

optimization, i.e., for a preliminary system design with prescribed net power output, minimize the total thermal conductance of evaporator and condenser could reduce the total cost, considering the investment cost is mainly related to the areas of heat exchangers.

In recent years, the GA method has been extensively applied to solve both single-objective and multi-objective optimization problems in thermal systems [24–26], because it could handle with the nonlinear problems. Therefore, in this study, based on the energy flow model, the GA method is employed to realize different optimizations of the ORC system.

4.1. Operation optimization

For a typical ORC system shown in Fig. 1, net power output and thermal efficiency are two common performance evaluation criteria, which could be individually optimized. However, they are conflicting criteria that cannot reach maximum simultaneously. Therefore, multi-objective optimization via GA is conducted to provide a set of non-dominated Pareto optimal solutions (Pareto frontier) to show the trade-offs between these two objectives. Each point at the Pareto frontier stands for a certain weight. After that, the TOPSIS method [43], one of the widely used multi-criteria decision analysis methods, is applied to select the final optimal point.

Considering the variation of the mass flow rate of cooling water would directly affect the power consumption of cooling water pump, thus, it could be simply calculated by

$$W_{p,w} = m_w g H_w, \tag{31}$$

where g is the gravitational acceleration and H_w is the pump head of cooling water. Taking the power consumption of cooling water pump into consideration, the net power output and the thermal efficiency then could be expressed as

$$W_{net} = W_t - W_p - W_{p,w}, \tag{32}$$

$$\eta = \frac{W_t - W_p - W_{p,w}}{Q_{e,1} + Q_{e,2} + Q_{e,3}}. \tag{33}$$

Table 4 lists the working conditions and design parameters for the ORC system shown in Fig. 1, wherein, R245fa is taken as the working fluid and hot water is used as the heat source. It is well known that the inlet parameters of waste heat resource including mass flow rate and temperature have significant influences on the thermal performance of an ORC system. Therefore, Fig. 6 gives the Pareto frontiers calculated by GA solver in optimization tool of MATLAB and the corresponding TOPSIS solutions of the ORC system, where the inlet temperature of hot water keeps at 366 K and the mass flow rate of hot water is 0.4 kg s^{-1}, 0.8 kg s^{-1} and 1 kg s^{-1}, respectively. In this condition, the optimized m_f and m_w of all the points on the Pareto frontier are within the optimization range listed in Table 4. The top-left points represent that the thermal efficiency accounts for a relative larger weight in optimization, whereas, the bottom-right points reflect that the net power output is more weighted.

The major characteristic parameters at TOPSIS points under different hot water mass flow rates are listed in Table 5. When the mass flow rate of hot water increases from 0.4 kg s^{-1} to 1 kg s^{-1}, the net power output and thermal efficiency will increase by 11% and 1.3%, respectively. The corresponding mass flow rate of cooling water and working fluid, evaporation temperature, condensation temperature and PPTD of evaporator and condenser will all increase to different extents. It could be also observed that the Pareto frontier has a little change

Table 4
The working conditions and design parameters of the ORC system for operation optimization.

Working conditions	Symbol	Value/Range
Inlet temperature of cooling water, K	$T_{w,i}$	303
Inlet temperature of heat source, K	$T_{h,i}$	350, 358, 366
Mass flow rate of heat source, kg s^{-1}	m_h	0.4, 0.8, 1.0
Pump head of cooling water, m	H_w	12
Degree of superheat, K	ΔT_{sh}	2
Thermal conductance of evaporator, W K^{-1}	$(KA)_e$	1712
Thermal conductance of condenser, W K^{-1}	$(KA)_c$	1443
Design parameters		
Mass flow rate of cooling water, kg s^{-1}	m_w	[0.50, 1.30]
Mass flow rate of working fluid, kg s^{-1}	m_f	[0.04, 0.10]

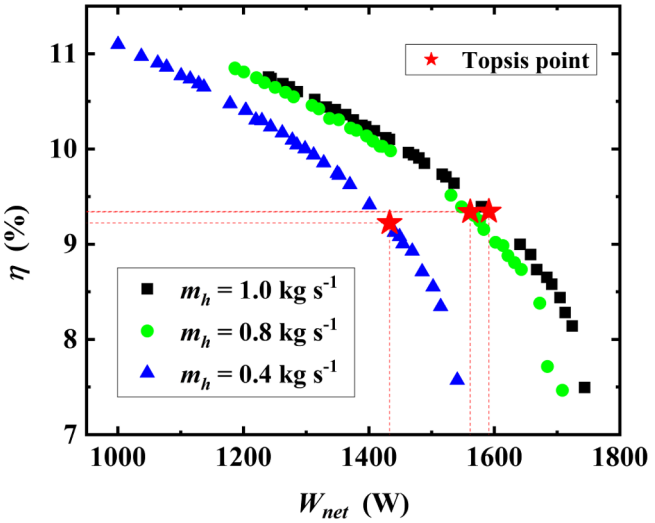

Fig. 6. The Pareto frontiers of the ORC system with different mass flow rates of hot water, when the hot water temperature is 366 K. (The star-marked points are selected by the TOPSIS method.)

Table 5
The major characteristic parameters at TOPSIS points with different mass flow rates of hot water.

Condition	Design parameters		Output parameters					
m_h (kg s^{-1})	m_w (kg s^{-1})	m_f (kg s^{-1})	W_{net} (W)	η (%)	T_c (K)	T_e (K)	$\Delta T_{pp,e}$ (K)	$\Delta T_{pp,c}$ (K)
1	0.859	0.081	1591	9.343	315.3	356.2	7.0	8.7
0.8	0.822	0.080	1562	9.339	315.2	356.0	6.6	8.4
0.4	0.758	0.074	1433	9.223	314.5	354.5	4.9	7.7

when hot water flow rate increases from 0.8 kg s^{-1} to 1 kg s^{-1}. That is because the net power output mainly depends on the evaporation and condensation temperature. When the hot water temperature is fixed, the upper limit of evaporation temperature and lower limit of condensation temperature are then determined. When the mass flow rate of hot water increases to a certain extent, it will have little impact on T_e and T_c.

Similarly, Fig. 7 shows the Pareto frontiers and its corresponding TOPSIS solutions, where the mass flow rate of hot water is fixed at 1 kg s^{-1}, and the inlet temperature of hot water is 350 K, 358 K and 366 K. The corresponding optimized parameters at TOPSIS point are listed in Table 6. With a 16 K increment in inlet temperature of hot water, the net power output and thermal efficiency will increase by 84% and 25%, respectively. The corresponding mass flow rate of cooling water and working fluid, evaporation temperature, condensation temperature and PPTD of evaporator and condenser will also increase. Compared Figs. 6 and 7, it is obvious that the impact of heat source inlet temperature on system performance is more remarkable than heat source mass flow rate. It could also be concluded that, it is necessary to properly allocate the mass flow rates of working fluid and cooling water to obtain the balance of more work output and higher system thermal efficiency. Moreover, the evaporation temperature, condensation temperature as well as the PPTD of evaporator and condenser vary with the boundary conditions of the system in each optimization.

4.2. Design optimization

The cost of heat exchangers is determined by heat transfer areas, and it accounts for a large portion of the total investment cost, which is a major concern in designing an ORC system [14]. Therefore, we take minimizing the total thermal conductance of evaporator and condenser as the objective to optimize a system with fixed design requirements, namely, net power outputs. It is worth to mention that the types of evaporator and condenser are unknown here. Therefore, the variations of the heat transfer coefficients which could be calculated by the empirical correlations are not considered. Based on the energy flow model, the optimization could also be readily implemented by single-objective GA.

Still using R245fa as the working fluid and hot water as the heat source, the working conditions and design parameter of the ORC system are listed in Table 7. When the required W_t is determined, Q_c, Q_e and W_{net} are then all fixed, and consequently one working fluid flow rate will correspond to one total thermal conductance. Fig. 8 shows the variation of minimum total thermal conductance and optimal mass flow rate of R245fa versus the required net power output. With the increase of net power output, the minimum total thermal conductance rises with an increasing slope, while the mass flow rate of working fluid decreases. When the net power output increases by 14.9%, the total thermal conductance will increase by 54.3% and the working fluid flow rate will only reduce by 8.7%. It indicates that thermal conductance has the major impact on the system performance, and a larger required net power output needs more heat transfer area rather than larger working fluid flow rate.

To further explore different effects of structural and operating parameters on system performance, the variations of the optimal parameters with different net power outputs are investigated. Fig. 9 depicts the optimal thermal conductance of evaporator and condenser as well as the relative ratio of them versus the net power output. Increasing required net power output results in a sharp increase in the thermal conductance of condenser while the thermal conductance of evaporator keeps almost constant. While, in the Fig. 10, as the net power output increases, the evaporation temperature remains almost invariable and the condensation temperature decreases approximately linearly, which means the condenser needs more heat transfer area. The reason for this phenomenon is that when the heat absorbed from evaporator is fixed, increasing the required net power output needs to decrease the heat emitted to the condenser, and consequently, the condensation temperature will also reduce. Then, a larger thermal conductance of condenser is imperative because the temperature difference between cooling water and the working fluid is reduced. From the ratio of thermal conductance of evaporator to condenser in Fig. 9, the contrast is more intuitive. When the net power output increases by

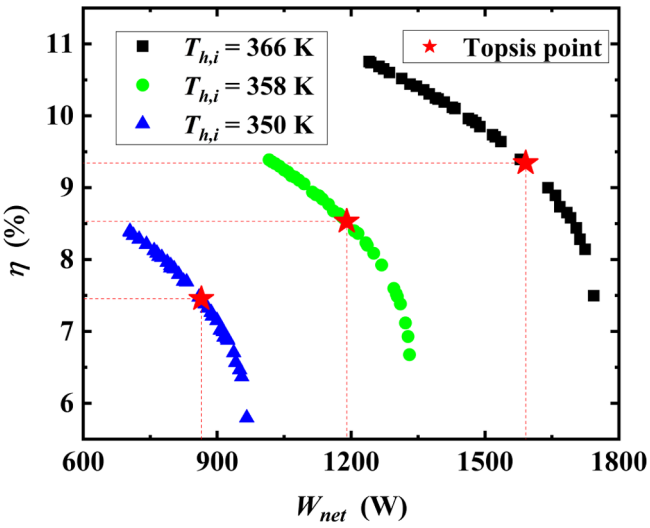

Fig. 7. The Pareto frontiers of the ORC system with different inlet temperatures of hot water, when the hot water flow rate is 1 kg s^{-1}. (The star-marked points are selected by the TOPSIS method.)

Table 6
The major characteristic parameters at TOPSIS points with different inlet temperatures of hot water.

Condition	Design parameters		Output parameters					
$T_{h,i}$ (K)	m_w (kg s^{-1})	m_f (kg s^{-1})	W_{net} (W)	η (%)	T_c (K)	T_e (K)	$\Delta T_{pp,e}$ (K)	$\Delta T_{pp,c}$ (K)
366	0.859	0.081	1591	9.343	315.3	356.2	7.0	8.7
358	0.671	0.067	1190	8.529	313.7	350.0	5.8	6.8
350	0.639	0.056	865	7.452	312.0	343.0	4.9	5.6

Table 7
The working conditions and design parameter of the ORC system for design optimization.

Working conditions	Symbol	Value/Range
Inlet temperature of heat source, K	$T_{h,i}$	366
Inlet temperature of cooling water, K	$T_{w,i}$	303
Mass flow rate of heat source, kg s^{-1}	m_h	1.0
Mass flow rate of cooling water, kg s^{-1}	m_w	2.2
Pump head of cooling water, m	H	12
Power consumption of working fluid pump, W	W_p	40.8
Work output of expander, W	W_t	2050–2350
Heat absorbed from evaporator, W	Q_e	20,600
Design parameter		
Mass flow rate of working fluid, kg s^{-1}	m_f	[0.09, 0.11]

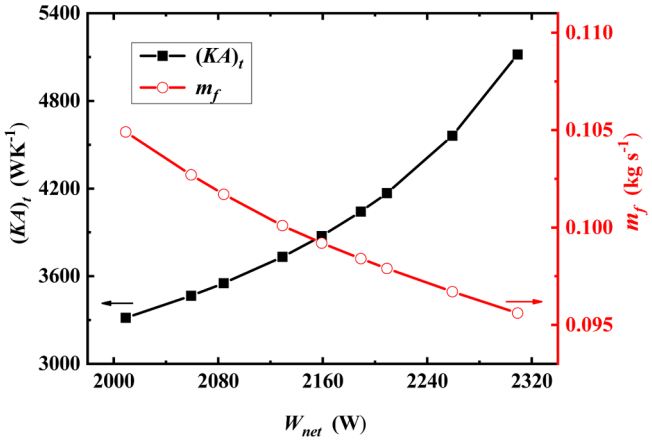

Fig. 8. The minimum total thermal conductance and the optimal mass flow rate of R245fa versus the net power output.

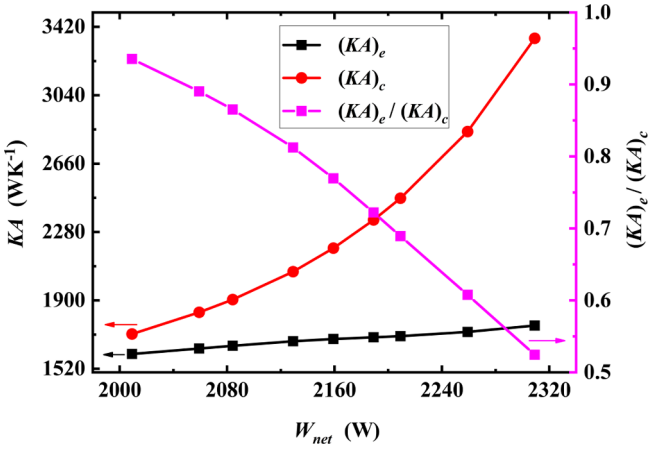

Fig. 9. The optimal thermal conductance of evaporator and condenser and the ratio of them versus the net power output.

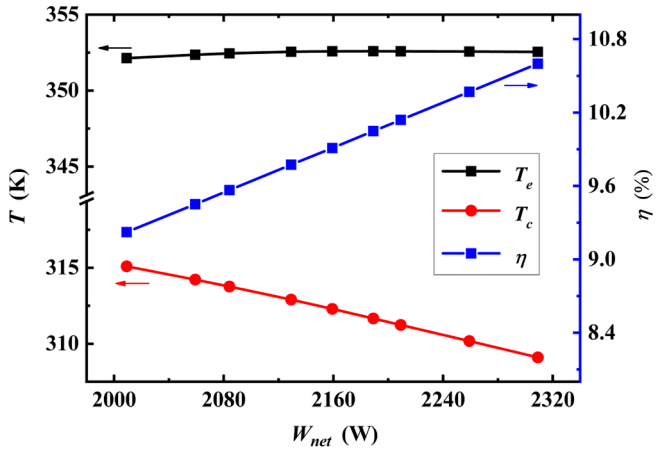

Fig. 10. The optimal evaporation temperature, condensation temperature and the thermal efficiency versus the net power output.

14.9%, the required thermal conductance of the condenser is nearly twice that of the evaporator. Fig. 10 also offers the variation of thermal efficiency versus net power output. The thermal efficiency is in direct proportion to the required net power output, which is also revealed by Eq. (33).

Fig. 11 gives the variations of corresponding PPTD of the evaporator and the condenser versus the net power output. The optimal PPTD of evaporator remains nearly invariable with the increase of net power output while the optimal PPTD of condenser monotonically decreases. Fig. 12 offers the optimal superheat degree of R245fa at the outlet of evaporator with different net power outputs. Obviously, the optimal superheat degree increases rapidly with the increase of net power output, which means, for different required net power outputs, the optimal values of degree of superheat remarkably vary. The different variation trends of these characteristic temperatures are also because of the fixed heat absorbed from the evaporator. For the evaporator, considering the evaporation temperature has little potential to increase due to the fixed Q_e, then only the allocation of heat absorbed in the preheating and the super-heating heat exchanger could be optimized by altering the superheat degree. Obviously, a higher temperature of R245fa entering into expander is in favor of obtaining more net power output. Meanwhile, for the condenser, decreasing the PPTD could reduce the condensation temperature and then increase the net power output. Therefore, in this condition, the mechanism of improving net

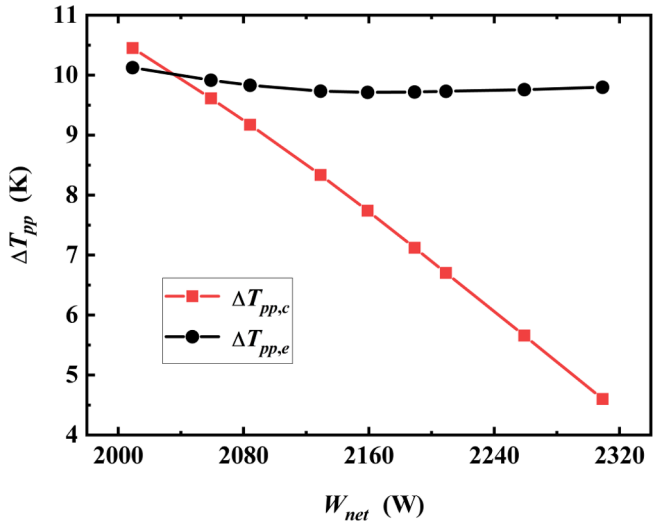

Fig. 11. The optimal PPTD of evaporator and condenser versus the net power output.

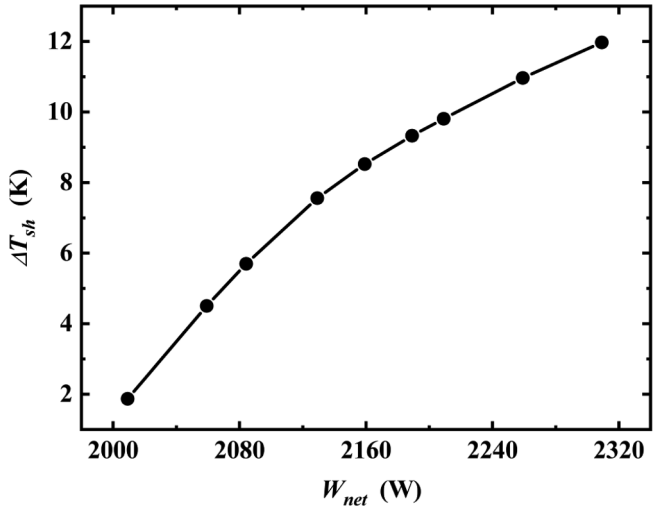

Fig. 12. The optimal superheat degree of R245fa at the outlet of evaporator versus the net power output.

power output is different in the evaporator and the condenser. Moreover, it is clear that all the intermediate temperatures also vary in each optimization. However, in the conventional design, limited by the modelling method, designers always need to empirically determine the evaporation temperature and the PPTDs in advance. The arbitrary fixed temperatures may lead to the failure of obtaining the optimal solutions.

From the above analysis, the optimal values of major characteristic parameters in the system, including evaporation temperature, condensation temperature, degree of superheat, and PPTDs always vary with different boundary condition or required net power outputs. Therefore, fixing these aforementioned parameters in system optimization is not rational.

5. Conclusion

From the system-oriented perspective, the energy flow model-based modeling method for an ORC system that synthetically considers fluid characteristics, heat transfer process and thermodynamic process is proposed. Then, the PPTDs, degree of superheat, evaporation and condensation temperature are not indispensable to be determined in advance of modeling.

Based on the validated model, operation optimizations for a certain ORC system with R245fa as the working fluid are conducted by multi-objective Genetic Algorithm (GA). The results offer two sets of Pareto frontiers and the optimal solutions selected by TOPSIS method under different heat source conditions. The heat source inlet temperature contributes substantially to improve performance. With a 16 K increment, the net power output and thermal efficiency will increase by 84% and 25%, respectively. The corresponding optimal PPTDs, evaporation and condensation temperature all increase. Whereas, the heat source flow rate has limited effect on optimizations, where, the obtained Pareto frontier of 0.8 kg s^{-1} nearly coincides with that of 1 kg s^{-1}.

Design optimizations to obtain minimum total thermal conductance with fixed inlet conditions are also implemented. When the net power output increases by 14.9%, the required total thermal conductance would increase by 54.3%, while the working fluid flow rate reduces by 8.7%. Besides, the corresponding thermal conductance of the condenser increases with a growing slope, while, the PPTD of the condenser and the condensation temperature decrease approximately linearly. Meanwhile, the thermal conductance, the PPTD of the evaporator and the evaporation temperature remain almost invariable during the optimizations. The results indicate that the operating parameters related to condenser effectively influence the optimizations, and such operating parameters as PPTDs and degree of superheat that should be fixed before modeling in the conventional modeling method vary in whether operation optimization or design optimization.

Declaration of Competing Interest

The authors declare that they have no known competing financial interests or personal relationships that could have appeared to influence the work reported in this paper.

Acknowledgment

This work was supported by the National Natural Science Foundation of China (Grant Nos. 51506061 & 51736004).

References

[1] Dong L, Liu H, Riffat S. Development of small-scale and micro-scale biomass-fuelled CHP systems – a literature review. Appl Therm Eng 2009;29:2119–26.
[2] Franco A, Villani M. Optimal design of binary cycle power plants for water-dominated, medium-temperature geothermal fields. Geothermics 2009;38:379–91.
[3] Rayegan R, Tao YX. A procedure to select working fluids for Solar Organic Rankine Cycles (ORCs). Renew Energy 2011;36:659–70.
[4] Delgado-Torres AM, García-Rodríguez L. Preliminary design of seawater and brackish water reverse osmosis desalination systems driven by low-temperature solar organic Rankine cycles (ORC). Energy Convers Manag 2010;51:2913–20.
[5] Nguyen TQ, Slawnwhite JD, Boulama KG. Power generation from residual industrial heat. Energy Convers Manag 2010;51:2220–9.
[6] Tian H, Shu G, Wei H, Liang X, Liu L. Fluids and parameters optimization for the organic Rankine cycles (ORCs) used in exhaust heat recovery of Internal Combustion Engine (ICE). Energy 2012;47:125–36.
[7] Wang XD, Zhao L. Analysis of zeotropic mixtures used in low-temperature solar Rankine cycles for power generation. Sol Energy 2009;83:605–13.
[8] Sun W, Yue X, Wang Y. Exergy efficiency analysis of ORC (Organic Rankine Cycle) and ORC-based combined cycles driven by low-temperature waste heat. Energy Convers Manag 2017;135:63–73.
[9] Li L, Ge YT, Luo X, Tassou SA. Experimental investigations into power generation with low grade waste heat and R245fa Organic Rankine Cycles (ORCs). Appl Therm Eng 2017;115:815–24.
[10] Mondejar ME, Ahlgren F, Thern M, Genrup M. Quasi-steady state simulation of an organic Rankine cycle for waste heat recovery in a passenger vessel. Appl Energy 2017;185:1324–35.
[11] Yang F, Zhang H, Yu Z, Wang E, Meng F, Liu H, et al. Parametric optimization and heat transfer analysis of a dual loop ORC (organic Rankine cycle) system for CNG engine waste heat recovery. Energy 2017;118:753–75.
[12] Muhammad U, Imran M, Lee DH, Park BS. Design and experimental investigation of a 1kW organic Rankine cycle system using R245fa as working fluid for low-grade waste heat recovery from steam. Energy Convers Manag 2015;103:1089–100.
[13] Yang SC, Hung TC, Feng YQ, Wu CJ, Wong KW, Huang KC. Experimental investigation on a 3kW organic Rankine cycle for low-grade waste heat under different operation parameters. Appl Therm Eng 2017;113:756–64.
[14] Wang ZQ, Zhou NJ, Guo J, Wang XY. Fluid selection and parametric optimization of organic Rankine cycle using low temperature waste heat. Energy 2012;40:107–15.
[15] Sun J, Li W. Operation optimization of an organic rankine cycle (ORC) heat recovery power plant. Appl Therm Eng 2011;31:2032–41.
[16] Li G. Organic Rankine cycle performance evaluation and thermoeconomic assessment with various applications part II: Economic assessment aspect. Renew Sustain Energy Rev 2016;64:490–505.
[17] Imran M, Park BS, Kim HJ, Lee DH, Usman M, Heo M. Thermo-economic optimization of Regenerative Organic Rankine Cycle for waste heat recovery applications. Energy Convers Manag 2014;87:107–18.
[18] Uusitalo A, Honkatukia J, Turunen-Saaresti T, Larjola J. A thermodynamic analysis of waste heat recovery from reciprocating engine power plants by means of Organic Rankine Cycles. Appl Therm Eng 2014;70:33–41.
[19] Song J, Gu C. Parametric analysis of a dual loop Organic Rankine Cycle (ORC) system for engine waste heat recovery. Energy Convers Manag 2015;105:995–1005.
[20] Siddiqi MA, Atakan B. Alkanes as fluids in Rankine cycles in comparison to water, benzene and toluene. Energy 2012;45:256–63.
[21] Li T, Zhu J, Zhang W. Cascade utilization of low temperature geothermal water in oilfield combined power generation, gathering heat tracing and oil recovery. Appl Therm Eng 2012;40:27–35.
[22] Bahadormanesh N, Rahat S, Yarali M. Constrained multi-objective optimization of radial expanders in organic Rankine cycles by firefly algorithm. Energy Convers Manage 2017;148:1179–93.
[23] Braimakis K, Karellas S. Energetic optimization of regenerative Organic Rankine Cycle (ORC) configurations. Energy Convers Manage 2018;159:353–70.
[24] Long R, Bao YJ, Huang XM, Liu W. Exergy analysis and working fluid selection of organic Rankine cycle for low grade waste heat recovery. Energy 2014;73:475–83.
[25] Fergani Z, Touil D, Morosuk T. Multi-criteria exergy based optimization of an Organic Rankine Cycle for waste heat recovery in the cement industry. Energy Convers Manage 2016;112:81–90.
[26] Zhai L, Xu G, Wen J, Quan Y, Fu J, Wu H, et al. An improved modeling for low-

grade organic Rankine cycle coupled with optimization design of radial-inflow turbine. Energy Convers Manage 2017;153:60–70.
[27] Peris B, Navarro-Esbrí J, Molés F, Mota-Babiloni A. Experimental study of an ORC (organic Rankine cycle) for low grade waste heat recovery in a ceramic industry. Energy 2015;85:534–42.
[28] Zhou N, Wang X, Chen Z, Wang Z. Experimental study on Organic Rankine Cycle for waste heat recovery from low-temperature flue gas. Energy 2013;55:216–25.
[29] Shu G, Zhao M, Tian H, Huo Y, Zhu W. Experimental comparison of R123 and R245fa as working fluids for waste heat recovery from heavy-duty diesel engine. Energy 2016;115:756–69.
[30] Hærvig J, Sørensen K, Condra TJ. Guidelines for optimal selection of working fluid for an organic Rankine cycle in relation to waste heat recovery. Energy 2016;96:592–602.
[31] Wang D, Ling X, Peng H, Liu L, Tao L. Efficiency and optimal performance evaluation of organic Rankine cycle for low grade waste heat power generation. Energy 2013;50:343–52.
[32] Roy JP, Mishra MK, Misra A. Performance analysis of an Organic Rankine Cycle with superheating under different heat source temperature conditions. Appl Energy 2011;88:2995–3004.
[33] Zhang H, Guan X, Ding Y, Liu C. Emergy analysis of Organic Rankine Cycle (ORC) for waste heat power generation. J Clean Prod 2018;183:1207–15.
[34] Di-Maria F, Micale C. Exergetic and economic analysis of energy recovery from the exhaust air of organic waste aerobic bioconversion by Organic Rankine Cycle. Energy Procedia 2015;81:272–81.
[35] Kim DK, Lee JS, Kim J, Kim MS, Kim MS. Parametric study and performance evaluation of an organic Rankine cycle (ORC) system using low-grade heat at temperatures below 80 °C. Appl Energy 2017;189:55–65.
[36] Chen Q, Hao JH, Zhao T. An alternative energy flow model for analysis and optimization of heat transfer systems. Int J Heat Mass Transf 2017;108:712–20.
[37] Guo ZY, Zhu HY, Liang XG. Entransy—a physical quantity describing heat transfer ability. Int J Heat Mass Transf 2007;50:2545–56.
[38] Zhao T, Min Y, Chen Q, Hao JH. Electrical circuit analogy for analysis and optimization of absorption energy storage systems. Energy 2016;104:171–83.
[39] Chen Q, Fu RH, Xu YC. Electrical circuit analogy for heat transfer analysis and optimization in heat exchanger networks. Appl Energy 2015;139:81–92.
[40] Hao JH, Ge WC, Chen Q, He KL, Luo HH, Zhou GP. Power flow method-based integrated modeling and optimization for building heat transport and gas refrigeration system. J Energy Eng 2018;144:04018060.
[41] Hu K, Chen L, Chen Q, Wang XH, Qi J, Xu F, et al. Phase-change heat storage installation in combined heat and power plants for integration of renewable energy sources into power system. Energy 2017;124:640–51.
[42] Xie P. Experimental study of low-temperature Organic Rankine Cycle [dissertation]. Wuhan (Hubei): Huazhong University of Science and Technology; 2016.
[43] Shukla A, Agarwal P, Rana RS, Purohit R. Applications of TOPSIS algorithm on various manufacturing processes: a review. Mater Today Proc 2017;4:5320–9.